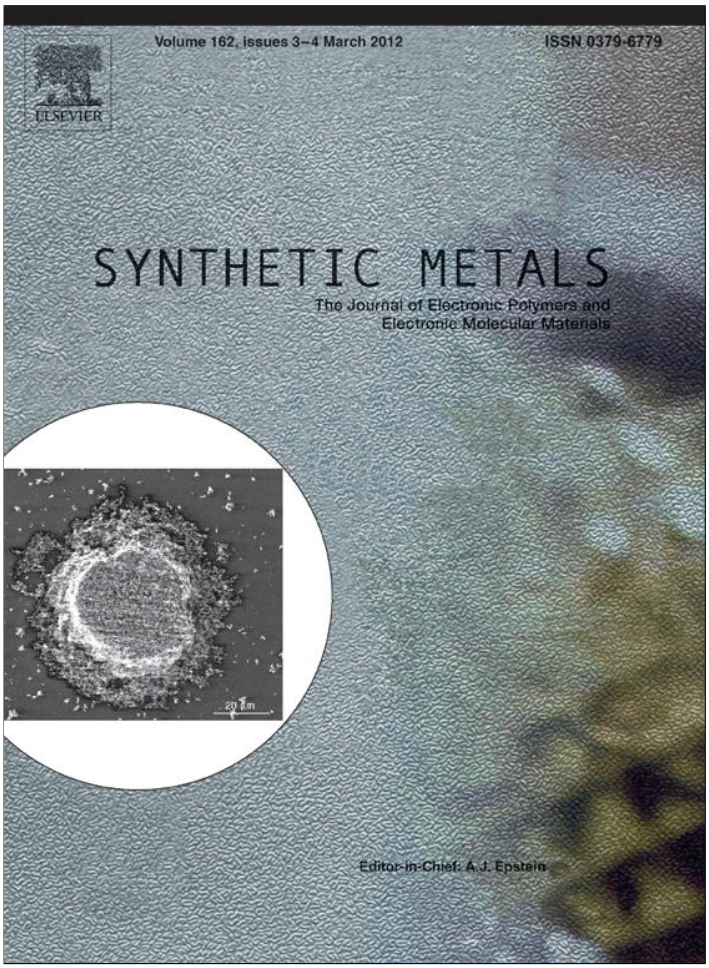

Synthetic Metals 162 (2012) 261–267

Contents lists available at SciVerse ScienceDirect

Synthetic Metals

journal homepage: www.elsevier.com/locate/synmet

3D metal–organic frameworks polymers of Pr(III) and Eu(III) with pyridine-2,6-dicarboxylic acid: Synthesis, structure and luminescent properties

Li-rong Yang*, Shuang Song, Huai-min Zhang, Wu Zhang, Lan-zhi Wu, Zhan-wei Bu, Tie-gang Ren

Institute of Molecule and Crystal Engineering, College of Chemistry and Chemical Engineering, Henan University, Kaifeng 475004, PR China

ARTICLE INFO

Article history:
Received 27 September 2011
Received in revised form
19 November 2011
Accepted 29 November 2011
Available online 10 January 2012

Keywords:
Metal–organic frameworks
Hydrothermal synthesis
Structure
Luminescent properties
Pyridine-2,6-dicarboxylic acid

ABSTRACT

Pyridine-2,6-dicarboxylic acid (H_2PDA) was used for the synthesis of two MOFs polymers $\{[Ln_2(PDA)_3(H_2O)_3]\cdot H_2O\}_n$ (Ln = Pr(**1**) and Eu(**2**)) with $Pr(NO_3)_3\cdot 6H_2O$ and $Eu(NO_3)_3\cdot 6H_2O$ under hydrothermal conditions and characterized by elemental analyses, IR spectroscopy, thermal analyses and single crystal X-ray diffraction. Both compounds crystallize in monoclinic system, space group $P21/c$. Both of the two compounds are isomorphous and isostructural. Different rings exist in the title compounds and form the 2D metal–organic framework. The 3D structures are constructed through covalent bonds and hydrogen bonds. The thermal decompositions have been predicted with the help of thermal analyses (TG and DTG). Furthermore, the luminescent properties of **2** were studied in the solution of DMF at room temperature.

1. Introduction

In the recent years, the exponential growth in the synthesis and characterization of metal–organic frameworks (MOFs) structures have been strongly stimulated by their potential application such as magnetism, catalysis, ionic exchange, sorption process and so on [1,2]. The MOFs containing lanthanide ions have the special (the word should better be deleted) magnetic, luminescent properties and more novel characters, which get more and more applications [3]. Trivalent lanthanide ions display some advantage factors of high and variable coordination number, favorable symmetry and entropy effects [4–6]. Therefore, the high dimensional polymers of lanthanide ions may be synthesized with multidentate ligands.

The MOFs including substitute pyridine ligands have been popular in the crystal engineering community as well as the materials chemists [7]. The pyridine-2,6-dicarboxylic acid (H_2PDA) is a multidentate (O,N,O) pyridine ligand, and it has been widely exploited to form metal derivatives that own versatile structure and interesting properties [8–11]. There are versatile coordination modes of H_2PDA ligand, not only because it contains several coordination atoms, but also it can be deprotonated with the suitable acidity and bind to metal ions as either a PDA^- or PDA^{2-} [12,13]. The PDA^{2-} can form a nine-coordination ties-chelate with lanthanide ions. The H_2PDA is an organic bridging ligand and it plays a double role in those compounds: firstly, it provides the skeletal backbone with metal ions and secondly it compensates the charge defect as a structure-directing molecule or template [14]. Based on these facts, a large number of MOFs with the pyridine-2,6-dicarboxylic acid ligand have being constructed [8,15].

The successful achievement of a lot of number of MOFs compounds has been realized by hydrothermal synthesis. The hydrothermal synthesis is an effective method for the construction of MOFs. We have been focused on the studies of pyridine dicarboxylate compounds of lanthanide and have been obtained some achievements [16,17]. In this paper, two novel metal–organic frameworks (MOFs) this word should be deleted structures have been synthesized of Pr(III) and Eu(III) with pyridine-2,6-dicarboxylic acid under hydrothermal conditions. The crystal structures of two compounds are similar. The 2D structures of compounds are formed by cyclization and 3D structures are connected by covalent bonds and hydrogen bonds. The luminescent properties and thermal analysis of two MOFs were studied.

2. Experimental

2.1. Reagents and general techniques

All chemicals are analytical grade and used without further purification. Elemental analysis was performed on a Perkin-Elmer 240C elemental analyzer. Infrared spectra were recorded in the 4000–400 cm^{-1} region using KBr pellets on an AVATAR 360 FT-IR spectrometer, the crystal structure was determined on a Bruker

* Corresponding author.
E-mail address: lirongyang@henu.edu.cn (L.-r. Yang).

0379-6779/$ – see front matter © 2011 Elsevier B.V. All rights reserved.
doi:10.1016/j.synthmet.2011.11.035

Smart CCD X-ray single-crystal diffractometer. Fluorescent data were collected on F-7000 FL Spectrophotometer at room temperature. The TG and DTG experiment were performed using a Perkin-Elmer TGA7 thermogravimeter. The heating rate was programmed to be 10 K min^{-1} with the protecting stream of N_2 flowing at 40 mL min^{-1}.

2.2. Syntheses

Syntheses of ***1***. An aqueous mixture of pyridine-2,6-dicarboxylic acid, praseodymium nitrate in molar ratio 1:1 were mixed in 10 mL water. The mixture was homogenized by stirring for 20 min, then transferred into 20 mL Teflon-lined stainless steel autoclave under autogenous pressure at 160 °C for 3 days. After cooling, green block crystals were isolated. Calc. For **1**, $C_{21}H_{15.50}N_3O_{15.25}Pr_2$ (%): C, 30.18; H, 1.87; N, 5.03. Found: C, 30.08; H, 1.95; N, 4.93. IR data (KBr pellet, cm^{-1}): 3431 (br), 1621 (s), 1585 (s), 1567 (s), 1444 (s), 1391(s), 1360(s), 1289 (w), 1277 (s), 1193 (w), 1177 (w), 1076 (m), 1017 (m), 927 (m), 828 (m), 761 (m), 730 (s), 695 (w), 659 (s), 582 (w), 524 (w), 469 (w), 433 (w).

Syntheses of ***2***. An aqueous mixture of pyridine-2,6-dicarboxylic acid, europium nitrate in molar ratio 1:1 were mixed in 10 mL water. The mixture was homogenized by stirring for 20 min, then transferred into 20 mL Teflon-lined stainless steel autoclave under autogenous pressure at 160 °C for 3 days. After cooling, yellow block crystals were isolated. Calc. For **2**, $C_{21}H_{15.50}N_3O_{15.25}Eu_2$ (%): C, 29.41; H, 1.82; N, 4.90. Found: C, 29.56; H, 1.91; N, 4.87. IR data (KBr pellet, cm^{-1}): 3447 (br), 1616 (s), 1571 (s), 1458 (m), 1446 (w), 1395 (m), 1359 (w), 1294 (w), 1279 (w), 1176 (w), 1076 (w), 1019 (w), 927 (w), 828 (w), 761 (w), 730 (m), 695 (m), 660 (m), 595 (w), 586 (w), 527 (w), 418 (w).

2.3. X-ray crystallographic determination

Single-crystal X-ray diffraction measurements of two MOFs polymers were carried out on a Bruker Smart CCD X-ray single-crystal diffractometer. Reflection data were at 291(2) K using graphite monochromated MoKα-radiation (λ = 0.71073 Å), $\omega/2\theta$ scan mode. All independent reflections were collected in a range of 1.93–25.00° for **1** and 1.90–25.00° for **2** and determined in the subsequent refinement. SADABS Multi-scan empirical absorption corrections were applied to the data processing [18]. The crystal structure was solved by direct methods and Fourier synthesis. Positional and thermal parameters were refined by the full-matrix least-squares method on F^2 using the SHELXTL software package [19]. The final least-square cycle of refinement gave $R_1 = 0.0213$, $wR_2 = 0.0537$ of **1** and $R_1 = 0.0196$, $wR_2 = 0.0506$ of **2**. The crystallographic data, selected bond lengths and bond angles for compounds are listed in Tables 1 and 2, respectively.

3. Results and discussion

3.1. IR spectra

Two MOFs compounds are stable in air and are sparingly soluble in DMF, but insoluble in other common organic solvents and water.

The IR spectra of two compounds are similar, some identical peaks (927, 828, 730 and 695 cm^{-1}) and very close peaks (3431, 1621, 1444, 1391 and 1289 cm^{-1} for **1** and 3447, 1616, 1446, 1395 and 1294 for **2**) are observed, the compound of **1** is selected in the following discussion. Most of the feature absorptions in the IR spectra are almost identical to the same ligands and structures [20–23]. The absorptions at 3431 cm^{-1} in high energy bonds (from 3500 to 2700 cm^{-1}) and 925 cm^{-1} in the low energy region for **1** are due to $\nu_{(H-O)}$ and $\delta_{(H-O)}$ of coordination water molecules [24]. In the IR spectra of **1**, all the bonds involving O—H motions

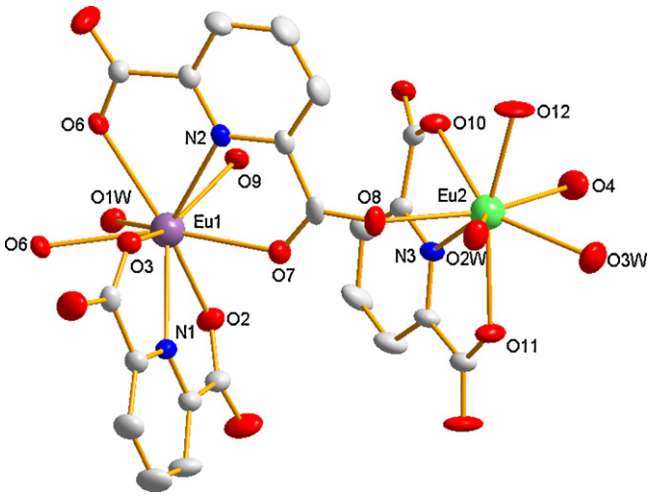

Fig. 1. Coordination environment of **2**; the asymmetric unit and the related coordination atoms are labeled and the hydrogen atoms are omitted for clarity: purple, Eu1; green, Eu2; red, O; blue, N; white, C. (For interpretation of the references to color in this figure legend, the reader is referred to the web version of the article.)

of the carboxylate ground are absent. For example, the characteristic carboxyl vibrations in the free H_2PDA ligand are found at 1702 cm^{-1} as a strong and broad vibration ($\nu_{(C=O)}$), and at 1331 and 1299 cm^{-1} is attributed to the $\nu_{(C-O)}$ stretching vibration, which transformed into the asymmetric $\nu_{as\ (COO^-)}$ at 1621 cm^{-1} and symmetric $\nu_{s\ (COO^-)}$ at 1391 cm^{-1} of **1**. The $\delta_{(O-C-O)}$ in-plane deformation vibration which occurs as a strong sharp bond at 701 cm^{-1} in the free ligand, but shift to higher frequency 730 cm^{-1} upon compound formation [25]. These results indicate deprotonation of the —COOH group and coordination to the metal ions. The bonds at 1585 and 761 cm^{-1} represent the characteristic skeleton vibrations of the pyridine ring. The weak bands between 582 and 433 cm^{-1} may be ascribed to $\nu_{(Pr-O)}$ and $\nu_{(Pr-N)}$.

3.2. Structural description

The asymmetric units of two MOFs are shown in Figs. 1 and 4(a). Each MOFs consists of two types metal ions, one is nine-coordination binding two tridentate PDA^{2-} ligands, two bridging carboxylate O atoms from neighbor metal ions and one coordinated water molecule (O1W), and the other is eight-coordination which includes one tridentate PDA^{2-}, three bridging carboxylate O atoms and two water molecules (O2W, O3W). In the case of **1**, the Pr—O and Pr—N lengths range from 2.353 to 2.574 Å and 2.595 to 2.643 Å, respectively. The average distance of Pr1—O is 2.453 Å, while Pr2—O is 2.527 Å, which is longer than the former. This result shows that the coordination environment of eight-coordination metal ion behaves more compact structures compared to those of the nine-coordination ones, and the same information also presents in **2** (Eu1—O (nine-coordination) is 2.471 Å and Eu2—O (eight-coordination) is 2.372 Å). The differences of lengths of Pr—O and Eu—O between eight-coordination and nine-coordination may be caused by steric hindrance derived from PDA^{2-} ligands. By comparison, the lengths of Pr—O and Pr—N in **1** are longer than those of Eu—O and Eu—N in **2**, which are potentially affected due to lanthanide contraction. Bond distances and bond angles involving the metal ion observation in the present work are consistent with the previous work for the lanthanide involved polymers [16,17,26].

The coordination modes of PDA^{2-} ligand, coordination fashions between metal ions, and the forming process of 3D packing structures of two MOFs polymers are very similar, so we focus on **1** in the following discussion.

Table 1
Summary of crystallographic data for **1** and **2**.

Data	1	2
CCDC deposit no.	821040	832604
Empirical formula	$C_{21}H_{15.50}N_3O_{15.25}Pr_2$	$C_{21}H_{15.50}N_3O_{15.25}Eu_2$
Formula weight	835.68	857.78
Temperature/K	296(2)	296(2)
Wavelength/Å	0.71073	0.71073
Crystal system	Monoclinic	Monoclinic
Space group	*P* 21/*c*	*P* 21/*c*
a/Å	10.9916(5)	10.9347(10)
b/Å	17.5108(8)	17.4867(15)
c/Å	13.4590(6)	13.2330(12)
α/°	90	90
β/°	100.9860(10)	101.5930(10)
γ/°	90	90
Z	4	4
Density(calculated)	2.183 g cm^{-3}	2.299 g cm^{-3}
F(000)	1610	1642
Crystal size/mm^3	0.45 × 0.36 × 0.31	0.48 × 0.38 × 0.26
Range for data collection/°	1.93–25.00	1.90–25.00
Limiting indices	$-13 \le h \le 6$, $-20 \le k \le 20$, $-15 \le l \le 15$	$-12 \le h \le 12$, $-20 \le k \le 15$, $-14 \le l \le 15$
Reflections collected/unique	12776/4478 [$R_{(int)}$ = 0.0179]	10170/4312 [$R_{(int)}$ = 0.0153]
Refinement method	Full-matrix least-squares on F^2	Full-matrix least-squares on F^2
Data/restraints/parameters	4478/0/381	4312/0/379
Goodness-of-fit on F^2	1.090	1.068
Volume/Å^3	2543.0(2)	2478.7(4)
Final *R* indices [$I > 2\sigma(I)$]	R_1 = 0.0213, wR_2 = 0.0537	R_1 = 0.0196, wR_2 = 0.0506
R indices (all data)	R_1 = 0.0235, wR_2 = 0.0545	R_1 = 0.0224, wR_2 = 0.0516
Largest diff. peak and hole/eÅ^{-3}	0.686 and −0.988	0.716 and −0.803

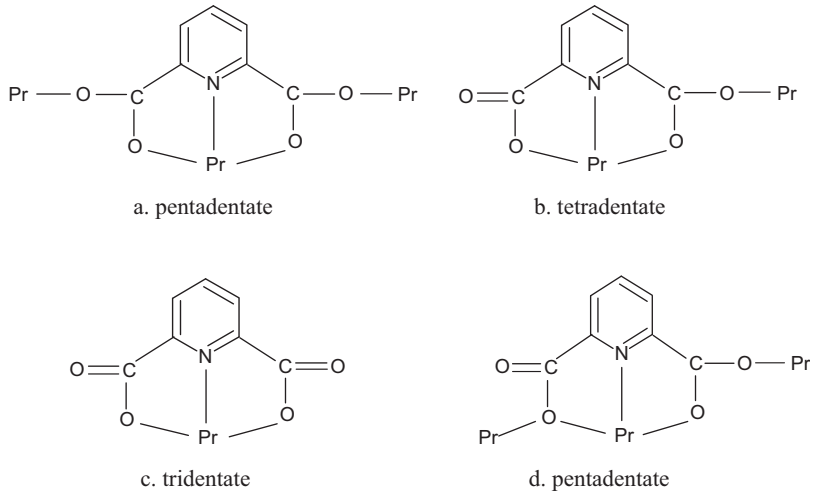

Scheme 1. Coordination modes of the H_2PDA ligand in compounds.

There are four types coordination modes of PDA^{2-} ligand in **1**, as shown in Scheme 1 and Fig. 2 (modes *a*–*d*). The eight-coordination ions of Pr1 links with three pentadentate (two of *a* mode and one *d* mode), one tetradentate (*b* mode), Pr2 is surrounded by one tridentate (*c* mode) and three pentadentate (one of *a* mode and two of *d* mode). The different coordination fashions around the metal ions are caused by tetradentate mode and two kinds of pentadentate modes. Coordination fashions between metal ions are described in Fig. 3, there are five praseodymium ions attach to Pr1A through O—C—O bridges, two Pr1 (Pr1B and Pr1C) and three Pr2 (Pr2A, Pr2C and Pr2D). Of four praseodymium ions around Pr2A, three Pr1 (Pr1A, Pr1D and Pr1E) are connected by O—C—O bridges and one of them forms diamond-shaped structure with Pr2B. The Ln···Ln distances in the MOFs structure of **1** have two distinct values. Firstly, the distance of Pr2A···Pr2B is 4.359 Å of diamond-shaped structure is shorter than others, so the short distances play an apparent role in stabilizing the MOFs polymers. Next, it's noteworthy that, several corresponding bond distances are approximatively equal in **1**

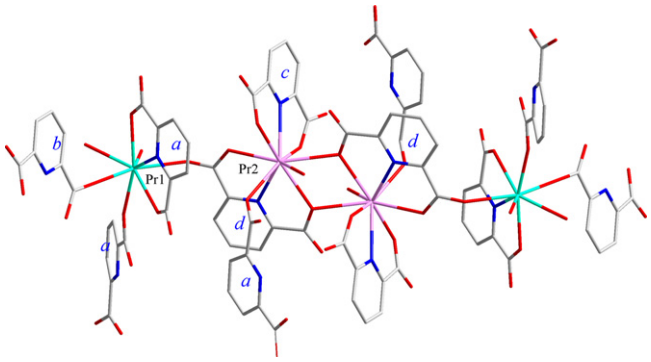

Fig. 2. The tagged crystal structure of **1** with coordination modes.

Table 2
Selected bond lengths (Å) and band angles (°) for **1** and **2**.

Bond lengths for **1**					
Pr(1)—O(4)	2.353(3)	Pr(1)—O(2 W)	2.558(2)	Pr(2)—O(7)	2.561(2)
Pr(1)—O(5)	2.367(2)	Pr(1)—N(1)	2.595(3)	Pr(2)—O(7) #1	2.574(2)
Pr(1)—O(9)	2.392(3)	Pr(2)—O(1)	2.463(2)	Pr(2)—O(1 W)	2.588(2)
Pr(1)—O(3)	2.479(2)	Pr(2)—O(11)	2.465(2)	Pr(2)—N(3)	2.605(3)
Pr(1)—O(3 W)	2.488(3)	Pr(2)—O(6)	2.490(2)	Pr(2)—N(2)	2.643(3)
Pr(1)—O(2)	2.534(2)	Pr(2)—O(10)	2.547(2)		
Bond lengths for **2**					
Eu(1)—O(9)	2.408(2)	Eu(1)—O(6)	2.536(3)	Eu(2)—O(11)	2.422(3)
Eu(1)—O(2)	2.410(3)	Eu(1)—N(1)	2.544(3)	Eu(2)—O(3 W)	2.441(3)
Eu(1)—O(7)	2.440(2)	Eu(2)—N(2)	2.577(3)	Eu(2)—O(10)	2.495(2)
Eu(1)—O(3)	2.503(2)	Eu(2)—O(12)	2.296(3)	Eu(2)—O(2 W)	2.507(3)
Eu(1)—O(1 W)	2.522(2)	Eu(2)—O(8)	2.310(3)	Eu(2)—N(3)	2.524(3)
Eu(1)—O(6) #1	2.527(2)	Eu(2)—O(4)	2.339(3)		
Bond angles for **1**					
O(4)—Pr(1)—O(5)	100.33(11)	O(1)—Pr(2)—O(11)	85.78(8)		
O(4)—Pr(1)—O(9)	85.31(11)	O(1)—Pr(2)—O(6)	79.10(8)		
O(5)—Pr(1)—O(9)	153.06(10)	O(11)—Pr(2)—O(6)	77.60(8)		
O(4)—Pr(1)—O(3)	162.15(9)	O(1)—Pr(2)—O(10)	140.96(8)		
O(5)—Pr(1)—O(3)	89.63(10)	O(11)—Pr(2)—O(10)	123.81(8)		
O(9)—Pr(1)—O(3)	92.51(10)	O(6)—Pr(2)—O(10)	83.13(8)		
O(4)—Pr(1)—O(2)	72.91(9)	O(1)—Pr(2)—O(7)	83.98(7)		
O(5)—Pr(1)—O(2)	78.55(9)	O(11)—Pr(2)—O(7)	155.02(8)		
O(9)—Pr(1)—O(2)	78.03(9)	O(6)—Pr(2)—O(7)	122.37(8)		
O(3)—Pr(1)—O(2)	124.00(8)	O(10)—Pr(2)—O(7)	76.69(7)		
O(4)—Pr(1)—N(1)	134.03(9)	O(1)—Pr(2)—O(7) #1	129.70(7)		
O(5)—Pr(1)—N(1)	77.63(9)	O(11)—Pr(2)—O(7) #1	107.12(8)		
O(9)—Pr(1)—N(1)	79.63(10)	O(6)—Pr(2)—O(7) #1	150.53(8)		
O(3)—Pr(1)—N(1)	62.42(8)	O(10)—Pr(2)—O(7) #1	70.00(8)		
O(2)—Pr(1)—N(1)	61.58(8)	O(7)—Pr(2)—O(7) #1	63.81(9)		
O(6)—Pr(2)—N(2)	61.74(8)	O(1)—Pr(2)—N(3)	140.98(8)		
O(10)—Pr(2)—N(2)	70.75(8)	O(11)—Pr(2)—N(3)	62.43(8)		
N(3)—Pr(2)—N(2)	116.35(9)	O(6)—Pr(2)—N(3)	72.71(8)		
O(1)—Pr(2)—N(2)	70.21(8)	O(10)—Pr(2)—N(3)	61.50(8)		
O(11)—Pr(2)—N(2)	135.49(8)	O(7)—Pr(2)—N(3)	134.07(8)		
O(7)—Pr(2)—N(2)	60.68(8)	O(7)#1—Pr(2)—N(3)	83.68(8)		
O(7)#1—Pr(2)—N(2)	117.12(8)	O(1 W)—Pr(2)—N(3)	116.46(8)		
Bond angles for **2**					
O(9)—Eu(1)—O(2)	83.51(9)	O(12)—Eu(2)—O(8)	100.72(11)		
O(9)—Eu(1)—O(7)	78.66(8)	O(12)—Eu(2)—O(4)	83.98(11)		
O(2)—Eu(1)—O(7)	76.74(9)	O(8)—Eu(2)—O(4)	152.12(10)		
O(9)—Eu(1)—O(3)	140.98(8)	O(12)—Eu(2)—O(11)	159.19(9)		
O(2)—Eu(1)—O(3)	126.11(8)	O(8)—Eu(2)—O(11)	89.54(10)		
O(7)—Eu(1)—O(3)	84.12(9)	O(4)—Eu(2)—O(11)	95.41(10)		
O(7)—Eu(1)—O(6)#1	150.46(8)	O(12)—Eu(2)—O(10)	73.36(9)		
O(3)—Eu(1)—O(6)#1	70.58(8)	O(8)—Eu(2)—O(10)	78.83(9)		
O(7)—Eu(1)—O(6)	125.01(8)	O(4)—Eu(2)—O(10)	76.26(10)		
O(3)—Eu(1)—O(6)	76.67(8)	O(11)—Eu(2)—O(10)	126.80(8)		
O(6)#1—Eu(1)—O(6)	64.55(9)	O(12)—Eu(2)—N(3)	135.84(10)		
O(9)—Eu(1) —N(1)	140.21(9)	O(8)—Eu(2)—N(3)	77.21(10)		
O(2)—Eu(1)—N(1)	63.78(9)	O(4)—Eu(2)—N(3)	80.42(10)		
O(7)—Eu(1)—N(1)	72.51(9)	O(11)—Eu(2)—N(3)	63.92(9)		
O(3)—Eu(1)—N(1)	62.47(9)	O(10)—Eu(2)—N(3)	62.88(9)		
O(6)#1—Eu(1)—N(1)	82.17(9)	O(9)—Eu(1)—N(2)	70.22(9)		
O(6)—Eu(1)—N(1)	134.16(9)	O(2)—Eu(1)—N(2)	135.04(9)		
N(1)—Eu(1)—N(2)	117.23(9)	O(7)—Eu(1)—N(2)	63.01(9)		
O(6)#1—Eu(1)—N(2)	119.13(9)	O(3)—Eu(1)—N(2)	70.76(8)		
O(6)—Eu(1)—N(2)	62.03(8)				

Symmetry transformations of **1** used to generate equivalent atoms: #1: $-x+1, -y+1, -z+1$; #2: $-x+2, -y+1, -z+1$; #3: $x, -y+1/2, z-1/2$; #4: $x+1, y, z$; #5: $x, -y+1/2, z+1/2$; #6: $x-1, y, z$. Symmetry transformations of **2** used to generate equivalent atoms: #1: $-x, -y, -z+1$; #2: $x+1, y, z$; #3: $-x+1, -y, -z+1$; #4: $x, -y+1/2, z-1/2$; #5: $x-1, y, z$; #6: $x, -y+1/2, z+1/2$.

(6.278 Å for Pr1A···Pr2C and Pr2A···Pr1D; 6.738 Å for Pr1A···Pr2B and Pr1A···Pr2C; 6.830 Å for Pr1A···Pr2D and Pr2A···Pr1E), this behaviors also appear in **2**. These facts indicate that, the coordination surroundings of each group of Ln···Ln may be very similar. A structure unit is assembled from three types of rings by sharing O—C—O bridges in the framework of **1**. Three rings are 18-membered ring $Pr_4C_4O_{10}$ (ring 1) which contains a Pr_2O_2 diamond-shape, 16-membered ring $Pr_4C_4O_8$ (ring 2) and 24-membered ring $Pr_6C_6O_{12}$ (ring 3), respectively. The 2D layer structure was constructed by the arrangement of structure units along *X* and *Y* directions. And then, the layers are connected along *Z* direction via covalent bonds of Pr—O—C—O—Pr and hydrogen bonds among the coordinated water and carboxylate oxygen, thus, the 2D layer further develops into the 3D MOFs polymers (the data of hydrogen bond are listed in Table 3 and the forming process of 3D packing structures see Fig. 4). The formation process of 3D MOFs in **2** is similar to that as above mentioned.

3.3. Luminescent properties

The luminescent properties of **2** were studied in DMF (10^{-4} M) at room temperature (excited at 282 and 326 nm) are given in Figs. 5 and 6. For the compound there is not only a broad excitation band in the range 325–341 nm, but also several characteristic

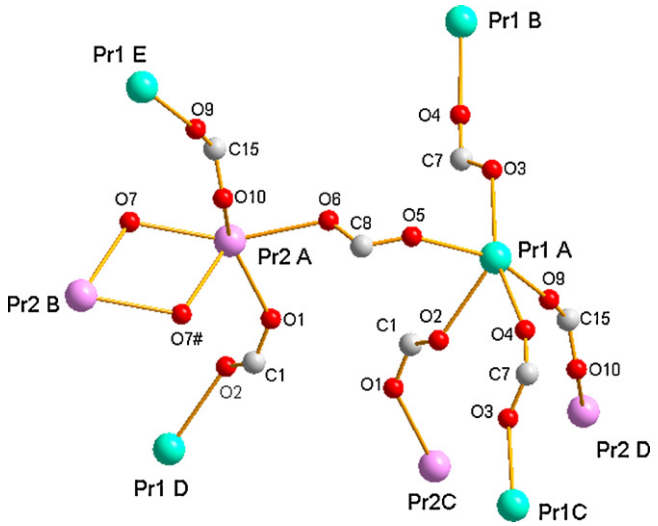

Fig. 3. Coordination layout between the metal ions of **1** and the non-coordination O and N atom with metal are omitted for clearness: green, Pr1; pink, Pr2; red, O; blue, N; white, C. (For interpretation of the references to color in this figure legend, the reader is referred to the web version of the article.)

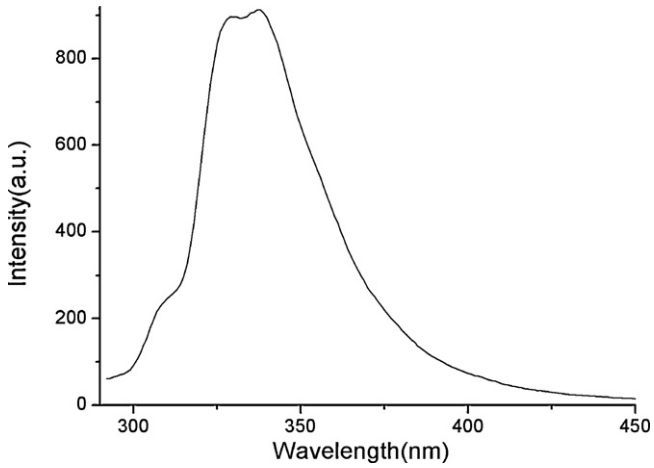

Fig. 5. Emission spectra of **2** in DMF (10^{-4} M) at room temperature (excited at 282 nm).

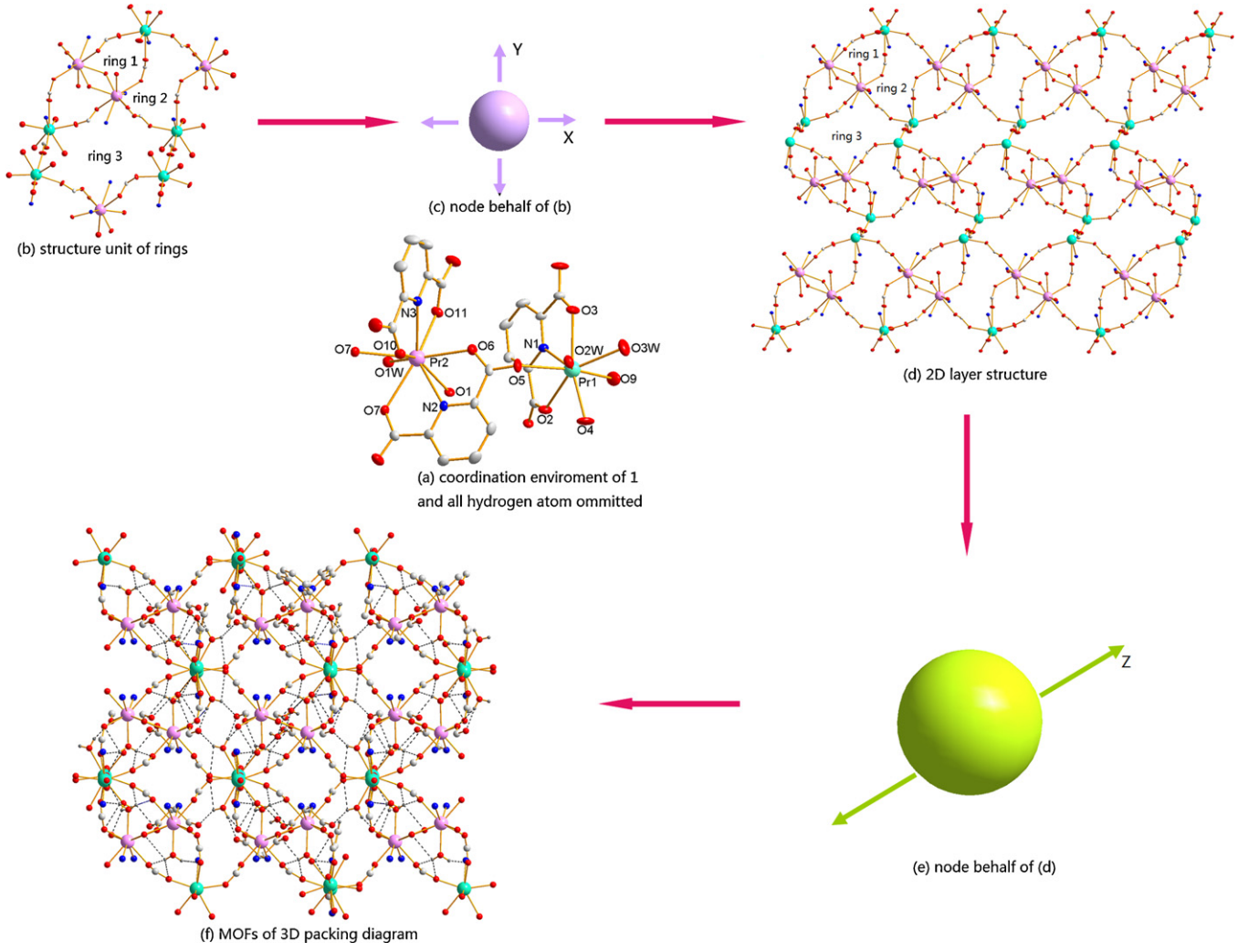

Fig. 4. The forming process of 3D MOFs structures for **1**: green, Pr1; pink, Pr2; red, O; blue, N; white, C. (For interpretation of the references to color in this figure legend, the reader is referred to the web version of the article.)

Table 3
Hydrogen bond geometry (Å/°) in **1** and **2**.

D—H···A	d(D—H)	d(H···A)	d(D···A)	∠(D—H···A)
Hydrogen bond for **1**				
O(4W)—H(4WB)···O(4W) #7	0.85	2.16	2.79(3)	130.4
O(3W)—H(3WB)···O(1W) #8	0.85	2.43	3.085(4)	134.0
O(3W)—H(3WB)···O(11) #8	0.85	2.25	2.991(4)	145.2
O(3 W)—H(3WA)···O(8) #9	0.85	2.43	2.915(4)	116.5
O(3W)—H(3WA)···O(4W) #9	0.85	1.99	2.801(13)	160.3
O(2W)—H(2WB)···O(12) #3	0.85	2.13	2.903(4)	150.5
O(2W)—H(2WA)···O(12) #8	0.85	1.95	2.787(4)	170.0
O(1W)—H(1WB)···O(10) #1	0.85	1.98	2.801(3)	162.7
O(1W)—H(1WA)···O(3) #10	0.85	2.59	3.147(3)	124.3
O(1W)—H(1WA)···O(2) #2	0.85	2.13	2.867(3)	144.0
Hydrogen bond for **2**				
O(1W)—H(1WA)···O(10)#3	0.85	2.12	2.850(4)	143.6
O(1W)—H(1WA)···O(11)#7	0.85	2.58	3.149(4)	125.1
O(1W)—H(1WB)···O(3)#1	0.85	1.94	2.769(4)	164.7
O(2W)—H(2WA)···O(1)#8	0.85	1.98	2.793(4)	159.5
O(2W)—H(2WB)···O(1)#4	0.85	2.22	3.001(4)	153.0
O(3 W)—H(3WA)···O(1W)#8	0.85	2.22	3.030(4)	158.3
O(3W)—H(3WA)···O(5)#9	0.85	2.50	2.981(5)	117.1
O(3 W)—H(3WB)···O(4W)#6	0.85	1.97	2.811(11)	168.4
O(4W)—H(4WB)···O(4W)#10	0.85	2.00	2.85(2)	175.6

Symmetry transformations of **1** used to generate equivalent atoms: #1: $-x+1$, $-y+1$, $-z+1$; #2: $-x+2$, $-y+1$, $-z+1$; #3: x, $-y+1/2$, $z-1/2$; #4: $x+1$, y, z; #5: x, $-y+1/2$, $z+1/2$; #6: $x-1$, y, z; #7: $-x+1$, $-y+1$, $-z$; #8: $-x+2$, $y-1/2$, $-z+3/2$; #9: $x+1$, $-y+1/2$, $z+1/2$; #10: $-x+2$, $y+1/2$, $-z+3/2$. Symmetry transformations of **2** used to generate equivalent atoms: #1: $-x$, $-y$, $-z+1$; #2: $x+1$, y, z; #3: $-x+1$, $-y$, $-z+1$; #4: x, $-y+1/2$, $z-1/2$; #5: $x-1$, y, z; #6: x, $-y+1/2$, $z+1/2$; #7: $-x+1$, $y-1/2$, $-z+3/2$; #8: $-x+1$, $y+1/2$, $-z+3/2$; #9: $x+1$, $-y+1/2$, $z+1/2$; #10: $-x+2$, $-y$, $-z$.

peaks are observed. The compound is excited at 282 nm because of a charge transfer band which can be assigned to the $\pi^* \rightarrow \pi$ transition of PDA^{2-} ligand [27,28] (see Fig. 5). This kind of charge transfer always occurs in Eu—O and Eu—N bonds in many complexes [26,29,30]. The emission spectra recorded in 335–630 nm of **2** is separated into two parts (see Fig. 6). The absorption in the range of 344–360 nm results from f–f transition of Eu^{3+} ion [31], and it is weaker than the $\pi^* \rightarrow \pi$ transition of ligand. The emission spectra at the range of 580–650 nm are contributed to transitions between the first excited state $^5D_0$ and the ground multiplet ^7F_J (J = 0–2) [27]. The symmetric forbidden emission $^5D_0 \rightarrow {}^7F_0$ at 581 nm can be found in **2**, which is strongly forbidden in regular octahedral structure [32,33]. $^5D_0 \rightarrow {}^7F_1$ (at 591 nm) is electric dipole transition, which is ruled by a magnetic dipole mechanism and being independent of the ligand field effects [34,35]. The band at 613 nm is

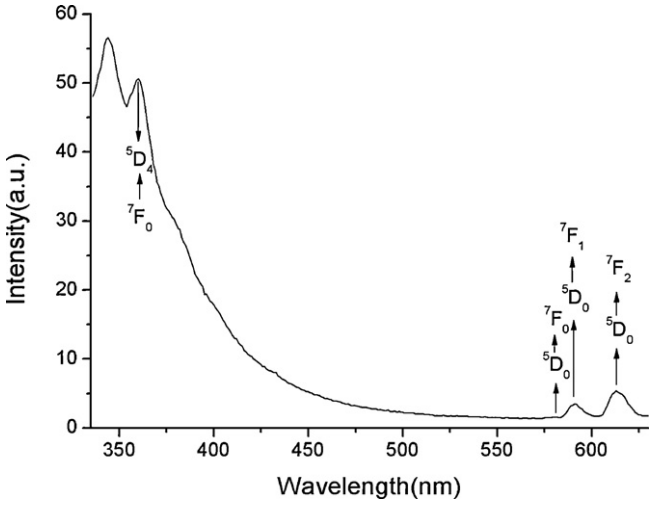

Fig. 6. Emission spectra of **2** in DMF (10^{-4} M) at room temperature (excited at 326 nm).

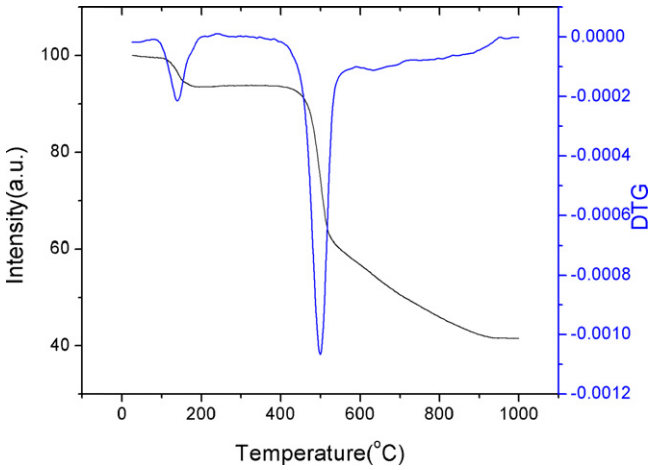

Fig. 7. TG and DTG curves of **1**.

contributed to $^5D_0 \rightarrow {}^7F_2$ transition. This band of $^5D_0 \rightarrow {}^7F_2$ transition is stronger than $^5D_0 \rightarrow {}^7F_1$ which indicate the highly polarizable chemical environment and the absence of version symmetry at the Eu(III) of the crystal [36,37]. All of the peaks are observed of **2**, which indicates the compound do not appear electron or phonon coupling at room temperature [31]. By comparison, the luminescent spectra of MOFs **1** are weak and covered by the peaks of solvent.

3.4. Thermal analysis

The thermal analyses of **1** and **2** are similar, and here we take **1** as example to descript. The TG and DTG curves of **1** are shown in Fig. 7, which indicate that the compound decomposes in two steps. The first weight loss stage has a decomposition temperature range of 110–456 °C with a weight loss of 5.30%, which corresponds to the loss of part of seven molecules of water (theoretical loss is 5.03%). On further heating, the material loses weight continuously during the second step, which has a decomposition temperature range of 456–930 °C with a weight loss of 53.17%, corresponding to the loss of two molecules of water and nine molecules of PDA^{2-} ligands (theoretical loss is 52.96%). The decomposition product was identified as Pr_6O_{11}. The observed weight (41.53%) was in good agreement with the calculated value (40.74%).

4. Conclusions

Two MOFs polymers $\{[Ln_2(PDA)_3(H_2O)_3]\cdot H_2O\}_n$ (Ln = Pr(**1**) and Eu(**2**)) were prepared and characterized. According to the data and discussion above, the structures of two compounds are very similar. Both the 3D frameworks are assembled from the structure units containing three types of rings via hydrogen bond and O—C—O bridges. The thermal decompositions of **1** have been predicted with the help of thermal analyses and emission spectra of **2** have been identified, respectively.

Supplementary material

CCDC-821040 and 832604 contain the supplementary crystallographic data for this paper. These data can be obtained free of charge via www.ccdc.cam.ac.uk/data_request/cif, or from the Cambridge Crystallographic Data Centre, 12 Union Road, Cambridge CB2 1EZ, UK; fax: +44 1223 336 033; or deposit@ccdc.cam.ac.uk.

Acknowledgments

This work was supported by the Natural Science Foundation of Henan Province, PR China (Nos. 2010B150005, 092102210172 and 2009B150005).

References

[1] S.K. Ghosh, P.K. Bharadwaj, Inorg. Chem. 42 (2003) 8250.
[2] B. Zhao, P. Cheng, X.Y. Chen, C. Cheng, W. Shi, D.Z. Liao, S.P. Yan, Z.H. Jiang, J. Am. Chem. Soc. 126 (2004) 3012.
[3] X.Q. Zhao, B. Zhao, Y. Ma, W. Shi, P. Cheng, Z.H. Jiang, D.Z. Liao, S.P. Yan, Inorg. Chem. 46 (2007) 5832.
[4] H.W. Hou, Y.L. Wei, Y.L. Song, Y.T. Fan, Y. Zhu, Inorg. Chem. 43 (2004) 1323.
[5] V.W. Manner, A.G. DiPasquale, J.M. Mayer, J. Am. Chem. Soc. 130 (2008) 7210.
[6] L.Y. Duan, Y.G. Li, F.C. Liu, E.B. Wang, X.L. Wang, C.W. Hu, L. Xu, J. Mol. Struct. 689 (2004) 269.
[7] M.K. Bhattacharyya, S.J. Bora, B.K. Das, J. Chem. Crystallogr. 38 (2008) 195.
[8] H. Hadadzadeh, A.R. Rezvani, M.K. Abdolmaleki, K. Ghasemi, H. Esfandiari, M. Daryanavard, J. Chem. Crystallogr. 40 (2010) 57.
[9] T.K. Prasad, S. Sailaja, M.V. Rajasekharan, Polyhedron 24 (2005) 1487.
[10] M.V. Kirillova, M.F.C. Guedes da Silva, A.M. Kirillov, J.J.R. Fraústo da Silva, A.J.L. Pombeiro, Inorg. Chim. Acta 360 (2007) 506.
[11] R.Q. Zou, X.H. Bu, M. Du, Y.X. Sui, J. Mol. Struct. 707 (2004) 11.
[12] V.C.R.Payne, O.S.C. Headley, R.T. Stibrany, P.T. Maragh, T.P. Dasgupta, A.M. Newton, A.A. Holder, J. Chem. Crystallogr. 37 (2007) 309.
[13] B.S. Parajón-Costa, O.E. Piro, R. Pis-Diez, E.E. Castellano, A.C. González-Baró, Polyhedron 25 (2006) 2920.
[14] C. Brouca-Cabarrecq, J.C. Trombe, J. Chem. Crystallogr. 39 (2009) 786.
[15] N.W. Alcock, G. Clarkson, P.B. Glover, G.A. Lawrance, P. Moore, M. Napitupulub, Dalton Trans. (2005) 518.
[16] L.R. Yang, S. Song, W. Zhang, H.M. Zhang, Z.W. Bu, T.G. Ren, Synth. Met. 161 (2011) 925.
[17] L.R. Yang, S. Song, W. Zhang, H.M. Zhang, Z.W. Bu, T.G. Ren, Synth. Met. 161 (2011) 1500.
[18] G.M. Sheldrick, SADABS: Empirical Absorption Correction Software, University of Göttingen, Institutfur Anorganische Chemieder Universitat, Tammanstrasse 4, D-3400 Göttingen, Germany, 1999.
[19] G.M. Sheldrick, SHELXTL: Version 5. Reference Manual, Siemens Analytical X-ray Systems, USA, 1996.
[20] C.L. Ma, J.K. Li, R.F. Zhang, D.Q. Wang, Inorg. Chim. Acta 358 (2005) 4575.
[21] B. Zhao, L. Yi, Y. Dai, X.Y. Chen, P. Cheng, D.Z. Liao, S.P. Yan, Z.H. Jiang, Inorg. Chem. 44 (2005) 911.
[22] A.C. Gonzalez-Baró, E.E. Castellano, O.E. Piro, B.S. Parajón-Costa, Polyhedron 24 (2005) 49.
[23] R.R. Tang, G.L. Gu, Q. Zhao, Spectrochim. Acta A 71 (2008) 371.
[24] A.C. González-Baró, R. Pis-Diez, O.E. Piro, B.S. Parajón-Costa, Polyhedron 27 (2008) 502.
[25] L. Wang, L.Y. Duan, E.B. Wang, D.Y. Xiao, Y.G. Li, Y. Lan, L. Xu, C.W. Hu, Transit. Metal Chem. 29 (2004) 212.
[26] P. Mahata, K.V. Ramya, S. Natarajan, Dalton Trans. (2007) 4017.
[27] T.Y. Zhu, K. Ikarashi, T. Ishigaki, K. Uematsu, K. Toda, H. Okawa, M. Sato, Inorg. Chim. Acta 362 (2009) 3407.
[28] J.W. Stouwdam, G.A. Hebbink, J. Huskens, F.C.J.M. van Veggel, Chem. Mater. 15 (2003) 4604.
[29] M. Li, L.J. Yuan, H. Li, J.T. Sun, Inorg. Chem. Commun. 10 (2007) 1281.
[30] K. Lunstroot, P. Nockemann, K.V. Hecke, L.V. Meervelt, K. Binnemans, K. Driesen, Inorg. Chem. 48 (2009) 3018.
[31] M.O. Rodrigues, N.B. da Costa Júnior, C.A. de Simone, A.A.S. Araújo, A.M. Brito-Silva, F.A.A. Paz, M.E. de Mesquita, S.A. Júnior, R.O. Freire, J. Phys. Chem. B 112 (2008) 4204.
[32] B. Zhao, X.Y. Chen, P. Cheng, D.Z. Liao, S.P. Yan, Z.H. Jiang, J. Am. Chem. Soc. 126 (2004) 15394.
[33] T.S. Li, W. Shang, F.L. Zhang, L.Y. Mao, C.Q. Tang, M.P. Song, C.X. Du, Y.J. Wu, Engineering 3 (2011) 301.
[34] B.L. An, K.W. Cheah, W.K. Wong, J.X. Shi, N.S. Xu, Y.S. Yang, M.L. Gong, J. Alloys Compd. 352 (2003) 143.
[35] Y.P. Cai, X.X. Zhou, Z.Y. Zhou, S.Z. Zhu, P.K. Thallapally, J. Liu, Inorg. Chem. 48 (2009) 6341.
[36] J.Q. Bao, C.H. Tang, R.R. Tang, J. Rare Earth 29 (2011) 15.
[37] Q.B. Bo, Z.X. Sun, W. Forsling, Cryst. Eng. Commun. 10 (2008) 232.